
This is an electronic reprint of the original article.
This reprint may differ from the original in pagination and typographic detail.

Sadi, Toufik; Radevici, Ivan; Kivisaari, Pyry; Oksanen, Jani
Electroluminescent Cooling in III-V Intracavity Diodes

Published in:
IEEE Transactions on Electron Devices

DOI:
[10.1109/TED.2018.2885267](https://doi.org/10.1109/TED.2018.2885267)

Published: 01/12/2018

Document Version
Peer-reviewed accepted author manuscript, also known as Final accepted manuscript or Post-print

Please cite the original version:
Sadi, T., Radevici, I., Kivisaari, P., & Oksanen, J. (2018). Electroluminescent Cooling in III-V Intracavity Diodes: Practical Requirements. *IEEE Transactions on Electron Devices*, 66(2), 963-968.
<https://doi.org/10.1109/TED.2018.2885267>

This material is protected by copyright and other intellectual property rights, and duplication or sale of all or part of any of the repository collections is not permitted, except that material may be duplicated by you for your research use or educational purposes in electronic or print form. You must obtain permission for any other use. Electronic or print copies may not be offered, whether for sale or otherwise to anyone who is not an authorised user.

Electroluminescent cooling in III-V intracavity diodes: practical requirements

Toufik Sadi, Ivan Radevici, Pyry Kivisaari and Jani Oksanen

Abstract—Recent studies of electroluminescent cooling in III-V structures demonstrate the need to understand better the factors affecting the efficiency of light emission and energy transport in light-emitting diodes (LEDs). In this work, we establish the physical and operational requirements for reaching the efficiencies needed for observing electroluminescent cooling in III-V intracavity double diode structures at high powers. The experimentally-validated modeling framework used in this work, coupling the drift-diffusion charge transport model with a photon transport model, indicates that the bulk properties of the III-V materials are already sufficient for electroluminescent cooling. Furthermore, the results suggest that the bulk power conversion efficiency of the LED in the devices, that allowed the experimentally measured record high coupling quantum efficiency of 70%, already exceeds 115%. However, as shown here, direct observation of electroluminescent cooling by electrical measurements still requires a combination of a more efficient suppression of the non-radiative surface recombination at the LED walls and the reduction of the detection losses in the photodetector of the intracavity structures.

Index Terms—Light-Emitting Diodes, Electroluminescent Cooling, Double Diode Structures, III-As.

I. INTRODUCTION

While the possibility of electroluminescent (EL) cooling was theoretically acknowledged already 60 years ago [1]–[3], quantitative and experimentally validated analysis of the requirements to observe it in practice are not yet available. The strategies for studying EL cooling (ELC) vary from thin-film light-emitting diodes (LEDs) [4], [5] and small band gap low power LEDs [6], [7], to high power visible LEDs [8] and intracavity devices [9]–[12]. The first three approaches deploy traditional light extraction methods with well known challenges, while the last one relies on a thermophotonic heat pump configuration [13], where the light is confined and used within a cavity with an essentially homogeneous refractive index. In this paper, we analyze the feasibility of observing ELC in the intracavity double diode structure (DDS) shown in Fig. 1, using a calibrated electro-optical model. We focus on the adverse role of non-radiative and surface recombination, and photodetector (PD) losses on device performance. Our results suggest that the present devices already have sufficient performance to exhibit ELC internally but reaching the net cooling threshold in practice will still necessitate overcoming

selected performance bottlenecks. The presented results will provide valuable insight on establishing the practical conditions for observing ELC at high powers.

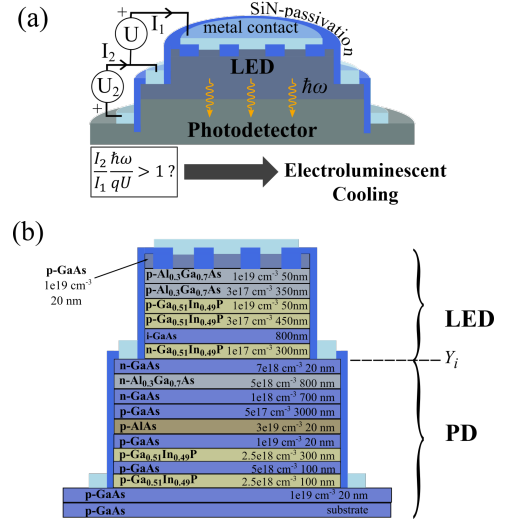


Fig. 1. (a) A cross sectional view of the simulated cylindrical intracavity DDS configuration, illustrating also the condition of the electrical detection of EL cooling. (b) The layer arrangement, materials and doping concentrations of the DDS.

II. THE DOUBLE DIODE SETUP

The DDS has been proposed as an attractive experimental setup for studying EL cooling. It encloses an InGaP/GaAs double heterojunction (DHJ) LED and a GaAs photodetector in a single cavity, as illustrated in Fig. 1. The DDS devices have been grown by metal-organic vapour phase and molecular beam epitaxy, with LED mesa diameters up to $\sim 1000\mu\text{m}$ [9], [14]. As the DDS configuration removes the need for light extraction, it can act as a useful intermediate research prototype in studying EL cooling. The PD in the DDS absorbs photons generated by injecting a current I_1 through the LED, resulting in a current I_2 through the short-circuited PD. Advantages of the DDS include bypassing the above mentioned light extraction issues, prevalent in typical LED setups, and minimized current crowding [14]. Additionally, the DDS allows straightforward characterization through measuring its coupling quantum efficiency (CQE), $\eta_{CQE} = I_2/I_1$. In the DDS setup, EL cooling can be directly observed if the power conversion efficiency (PCE) of the DDS $\eta_{PCE} = \eta_{CQE} \hbar\omega/qU$ is above unity. Here, U is the LED bias and $\hbar\omega$ is the average energy of the emitted photons.

Figure 2(a) further highlights the charge transport and energy exchange effects associated with electroluminescence,

Manuscript received September 17, 2018; revised November 21, 2018; accepted December 1, 2018. Date of publication December 18, 2018; date of current version January 22, 2019. This work was supported in part by the Academy of Finland and in part by the European Research Council through the Horizon 2020 Research and Innovation Program under Grant 638173. The review of this paper was arranged by Editor C.Surya. (Corresponding author: Toufik Sadi.)

The authors are with the Engineered Nanosystems Group, School of Science, Aalto University, FI-00076 Aalto, Finland (e-mail: toufik.sadi@aalto.fi). Digital Object Identifier 10.1109/TED.2018.28852

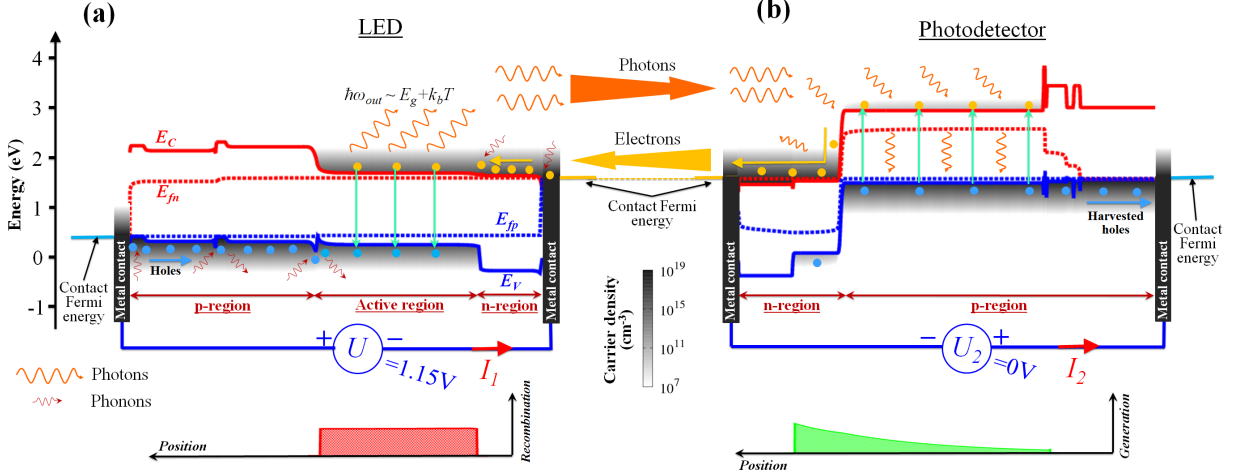


Fig. 2. (a) Schematic illustration of the current transport and carrier recombination in the LED, using its band diagram and recombination profiles calculated for a bias voltage $U = 1.15V$, which allows ELC. (b) The band diagram and generation profile of the photodetector (PD) excited by the luminescence from the LED. A hole current is harvested in the p-type contact, while the generated electrons are supplied back to the LED.

by showing an example band diagram and the corresponding recombination profile of an InGaP/GaAs DHJ LED biased at $\sim 1.15V$, which in our study will allow EL cooling after selected optimizations. Luminescence from the LED is additionally directly coupled to the built-in PD, whose band diagram is illustrated in Fig. 2(b). In the setup of Fig. 2, a suitable combination of a high CQE ($\sim 81\%$ or above) and an LED bias ($1.15V$) significantly below the bandgap of the active region (AR), results in a PCE above unity. This corresponds to the condition where heat absorption can overcome the internal heat generation leading to EL cooling. Indeed, in an ELC setup, the electrical excitation generally allows using bias voltages that are well below the bandgap voltage ($\sim 1.42V$). This is in contrast to photoluminescent (laser) cooling, in which the excitation power quickly falls when the excitation photon energy drops below the bandgap energy.

III. SIMULATION METHOD AND MEASUREMENTS

Charge transport is modelled by solving the three-dimensional drift-diffusion (DD) equations, calculating self-consistently the electrostatic potential, net recombination rates, densities and quasi-Fermi levels for electrons and holes [15], [16]. The recombination rates are determined using the ABC parameterized formula for the Shockley–Read–Hall (SRH), radiative and Auger recombination mechanisms [16]. The rates for interface and surface (non-radiative) recombination are calculated as described in [15]. The LED is biased in the customary manner while short-circuiting the PD. The total recombination in the LED active region (i-GaAs) is coupled to the total generation in the PD (GaAs) layers using an optical coupling constant. The generation profiles in the PD follow the Beer-Lambert law [15]. The coupling constant is evaluated by solving the radiative transfer equation [17], with the top-contact–cap-layer system reflectivity pre-calculated using the transfer matrix method [18]. The simulations are calibrated using the three point probe $I - V$ measurements [9], [14], biasing the LED with a voltage U and measuring the LED

current I_1 , and the current generated in the PD I_2 by the LED emitted photons.

IV. RESULTS AND DISCUSSION

In this work, the fundamental material parameters are primarily based on the available literature values, whereas the device specific parameters have been calibrated using experiments. A good agreement with experiments is obtained (see Fig. 3) using established values for the recombination parameters, including the recombination constants for radiative $B = 2 \times 10^{-10} cm^3 s^{-1}$ [19], [20] and Auger $C = 10^{-30} cm^6 s^{-1}$ [21] recombination processes, the recombination velocity $v_{sr} = v_{sr0} = 4 \times 10^5 cm/s$ at the mesa surfaces [22], and the recombination velocity at GaAs/InGaP interfaces $v_{int} = 1.5 cm/s$ [22]. For the SRH recombination constant A , we use a conservative value $3 \times 10^5 s^{-1}$ as compared to the best literature values [23]–[25], representing the upper limit for the model calibration sensitivity. Our previous work [9], [14], [15] suggests that the main DDS loss factors include non-radiative and surface recombination, as well as photodetection losses. Here, we study how improvements in selected device parameters affect the DDS efficiency. In section IV-A, we analyze the effect of non-radiative SRH and surface recombination on the LED, PD and DDS quantum efficiencies, by modifying A and v_{sr} from their reference values (A_0 and v_{sr0} , respectively). In section IV-B, we additionally assess the impact of recombination and other associated loss mechanisms on the photodiode quantum efficiency, by varying the thickness of the n-type GaAs layer in the PD from the reference value of 700nm. Finally, in sections IV-C–IV-D, we analyze the impact of recombination processes and device geometry on the power conversion efficiency of the DDS and the LED, and discuss the actions needed to reach the efficiency level required by EL cooling.

A. Quantum efficiency

Effect of surface recombination

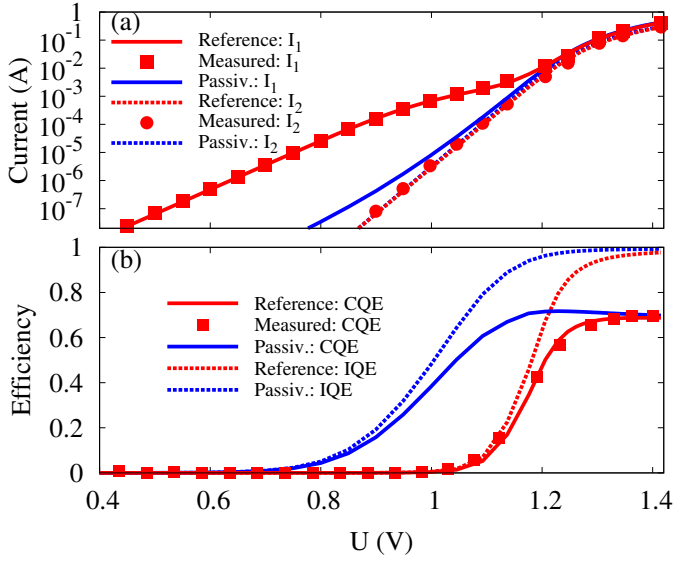


Fig. 3. The effect of surface passivation on the simulated (a) LED ($I_1 - U$) and photodiode ($I_2 - U$) characteristics, and (b) the corresponding LED IQE and DDS CQE as a function of the LED bias U . The lines in red show the characteristics for the reference structure (representing also the measurements of the real devices with strong surface recombination), and the lines in blue show the characteristics of the efficiently surface-passivated surface-recombination-free ($v_{sr} = 0$) structure. Measurement results are shown using data points for the reference DDS, indicating excellent agreement with simulations.

To illustrate how surface passivation is expected to affect the device characteristics, we show in Fig. 3 the LED, PD and DDS characteristics for two devices: (i) the measured and simulated data for the reference device and (ii) simulation data for an identical (but passivated) device without surface recombination, as obtained by setting v_{sr} at the mesa walls to zero. In Fig. 3(a), the LED and PD currents, as a function of the LED bias U , are shown for both devices. With $v_{sr} = 0$, the LED current at small biases is dramatically reduced becoming comparable to the photocurrent I_2 , indicating a substantial improvement in the efficiency. In contrast, passivation has no effect on the photocurrent. Fig. 3(b) shows the effect of passivation on the LED internal quantum efficiency (IQE) η_{IQE}^{LED} and the DDS CQE η_{CQE} , as a function of LED bias. Fig. 3(b) clearly highlights how passivation dramatically improves the LED IQE and (consequently) the DDS CQE. Fig. 3 therefore suggests that non-radiative recombination at the outer surfaces of the AR is the main mechanism driving current at low injection ($U < 1.1V$). In addition to reducing the CQE throughout the studied operating range, surface recombination shifts the peak CQE to higher LED biases, making the observation of ELC (via the condition $\eta_{PCE} > 1$) more challenging. Fortunately, it is to be expected that, once identified, this mechanism can be efficiently suppressed by available surface passivation techniques and improvements in the device structure.

Effect of material quality

Fig. 4 compares how the material quality of the device affects the CQE, and the LED and PD IQEs of the reference device and the corresponding passivated device. Fig. 4(a) shows that, for a fully-passivated surface, improving the material quality (lowering A) substantially increases the peak

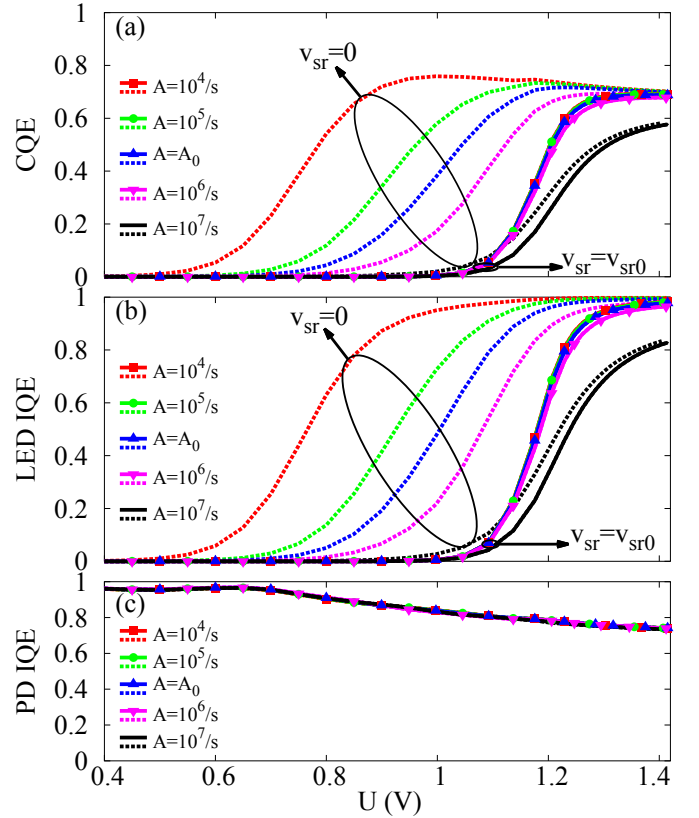


Fig. 4. The (a) CQE, (b) LED IQE, and (c) PD IQE, as a function of U and A , for the unpassivated ($v_{sr} = v_{sr0}$) reference device (solid/symbols) and the fully passivated ($v_{sr} = 0$) device (dashed).

CQE and moves the peak value of the CQE towards lower biases. For the reference device with very strong surface recombination ($v_{sr} = v_{sr0} = 4 \times 10^5 \text{cm/s}$), the improvement in the CQE is clearly visible only when A has a high value of 10^7s^{-1} . Reducing A below A_0 for the unpassivated (reference) device therefore has only a very limited effect on the CQE, which saturates at a peak value of $\sim 70\%$ independent of A if $A \leq A_0$. This behaviour shows that, in reality, the A parameter in our devices may in fact be smaller than the presently used worst case reference value of $A = A_0 = 3 \times 10^5 \text{s}^{-1}$. A similar trend is also clearly visible in the LED IQE, shown in Fig. 4(b), where A has a substantial effect, especially at low biases, only when surface passivation is applied. At larger biases, where the surface current saturates, the IQE still clearly increases with bias for a large A , but does not significantly improve as A is lowered to below the $A = A_0$ level. Fig. 4(c) shows the IQE of the PD as a function of the LED bias. While the IQE of the PD is near unity at low biases, it significantly decreases towards higher biases. This introduces a very harmful mismatch between the regions of peak efficiency of the PD and the LED, as analyzed in more details shortly. Neither the surface passivation nor the material quality of the PD have a visible effect on the PD efficiency within the studied range of A .

B. Origin of the PD losses

As observed in Fig. 4, the performance of the PD in the reference DDS has a profound effect on the CQE at biases

where the LED operates efficiently. To understand the origin of these performance issues and to eliminate it, we analyze the PD losses in more detail. As shown in the example band diagram of the PD in Fig. 2(b), the electron and hole populations in the GaAs layers of the PD can be substantially larger than the respective equilibrium values. Naturally, this can also lead to recombination in these layers. To assess its impact, we show in Fig. 5 a one-dimensional (1D) distribution of the recombination rates in the DDS along the vertical axis at the center of the mesa structure, at a bias $U = 1.15V$. The data is shown for a 700nm n-type GaAs layer in the PD, corresponding to the geometry of the reference device, as well as for a similar structure but with a 200nm n-type layer. Fig. 5 illustrates that the recombination in the PD predominantly takes place in the n-GaAs layer, and that the original DDS with a thick n-GaAs PD layer experiences a larger total recombination than the structure with a thinner n-GaAs layer. This undesirable recombination is a consequence of the accumulation of photogenerated holes in the n-GaAs layer of the PD, due to the very low mobility of holes as compared to electrons and the high electron-hole generation rate in this layer. This results in the reduction of the net photo-generated current (I_2) across the short-circuited PD, leading to lower CQEs. To quantify the differences caused by the n-type GaAs layer in more detail, Fig. 6 compares the CQE, and the LED and PD IQEs for layer thicknesses of 100nm, 200nm and 700nm. The CQE and the PD IQE are improved visibly at lower thicknesses, and the passivated device exhibits the highest peak CQE for thin n-layers. Indeed, according to the results, using a thinner n-type layer clearly improves the PD IQEs at large biases and hence increases the peak CQEs (reaching $\sim 90\%$ or higher). The LED IQE is obviously unaffected by the PD geometry.

C. Power conversion efficiency

Figures 7 and 8 analyze how various non-radiative recombination processes affect the power conversion efficiency of the LED and the DDS when the main recombination parameters and the PD geometry is varied. Figure 7 shows the PCE of the DDS and the internal power conversion efficiency (IPCE) representing the PCE of the LED itself, for the unpassivated reference device and the passivated ($v_{sr} = 0\text{cm/s}$) device, with selected A values. The IPCE is calculated by $\eta_{IPCE} = \eta_{IQE}^{LED} \hbar\omega/qU$, where η_{IQE}^{LED} is the IQE of the LED. Figure 7(a) indicates that lower v_{sr} and A give globally a higher PCE with the peak value shifting towards lower biases, similar to the trend observed for the CQE in Fig. 4. Figure 7(a) clearly shows that reducing v_{sr} close to zero can remarkably increase the PCE of the DDS by almost 15%, as compared to the reference device. This shows that just eliminating the surface recombination would bring the PCE of the DDS already very close to (or even above) unity, for fully feasible values of A in the range $10^4\text{s}^{-1} - A_0$, even without additional device optimization. Fig. 7(b) shows the corresponding analysis for the IPCE of the LED, where eliminating the surface recombination directly increases the IPCE to approximately 116%, for the reference (conservative)

$A = A_0$. This clearly illustrates that the bulk properties of the LED materials are sufficient for achieving EL cooling. In addition, the IPCE of the reference device also reaches $\sim 105\%$ even without any surface passivation.

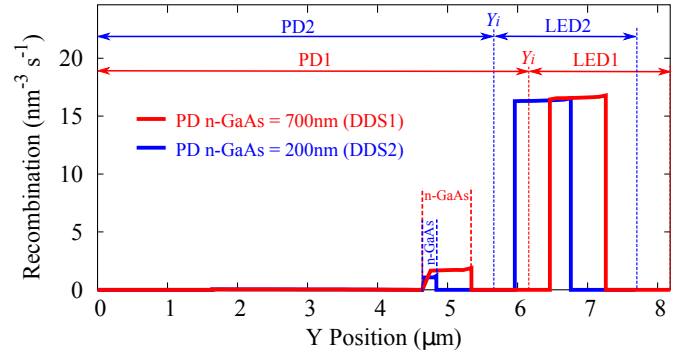


Fig. 5. 1D recombination profiles along a vertical cut in the middle of the mesa, for a device with a 200nm (in blue) and 700nm (in red) n-type GaAs layer in the PD. The LED and PD regions, as illustrated in Fig. 1, are denoted here. The n-GaAs PD layers are also shown, where undesirable recombination occurs. The bottom PD contact is at $y = 0$.

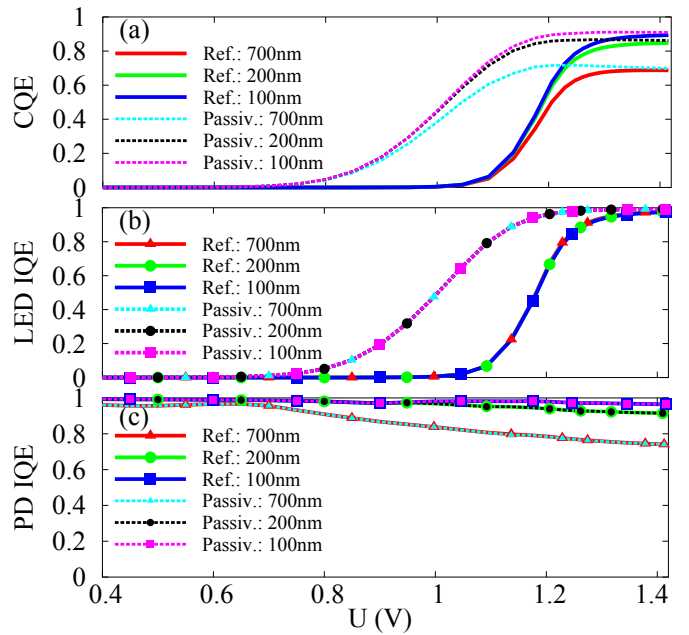


Fig. 6. (a) The CQE, (b) the LED IQE, and (c) the PD IQE as function of the LED bias U , for the PD n-type GaAs layer thicknesses of 100nm, 200nm and 700nm. The results for the reference structure are drawn with solid lines while dashed lines are used for the passivated structure.

D. Requirements for direct ELC observation

As seen above, applying one type of optimization (material improvement, passivation or PD optimization) alone may not be sufficient for directly observing ELC in the DDS, especially for conservative A values ($A \geq A_0$). On the other hand, combining two optimizations, such as material improvement and surface passivation as observed in Fig. 7 can result in PCE values that are well above unity. To assess the other combinations leading to PCE values in excess of unity, and hence

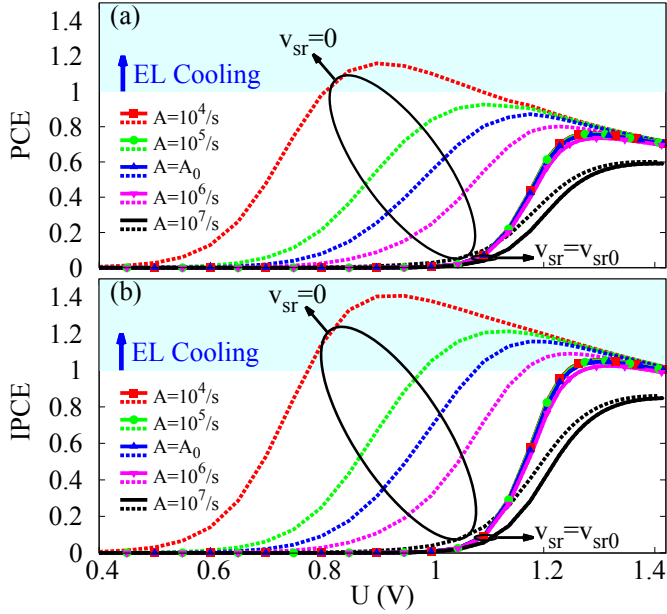


Fig. 7. Dependence of (a) the PCE of the DDS and (b) the predicted IPCE (PCE of the LED), as function of the LED bias U , for selected values of A , for the reference device ($v_{sr} = v_{sr0}$ – solid lines/symbols) and the surface passivated device ($v_{sr} = 0$ – dashed lines).

the possibility of observing EL cooling, we show in Figs. 8(a) and (c) the extrinsic PCE (EPCE, corresponding to the directly measured PCE involving an additional resistive loss of $\sim 3.75\Omega$ in the measurement setup) of the DDS, the PCE of the DDS (without the measurement resistance) and the PCE of the LED alone (IPCE), for the structure with a thin absorber layer (100nm), with and without passivated mesa edges, as function of both LED bias U and the input power ($I_1 \times U$). The EPCE of the DDS is calculated as $\eta_{EPCE} = \eta_{CQE} \hbar\omega / qU_1$, with U_1 including the external resistive losses associated with the measurement setup. For the thin photodetector structure with surface passivation, all of the PCEs have peak values higher than unity, with maxima 106%, 108% and 116% for the EPCE, PCE, and IPCE, respectively. This indicates that EL cooling can be directly observed in a passivated device when using a conservative A value $A_0 = 3 \times 10^5 s^{-1}$, even when the external resistive losses from the measurement setup are not eliminated. Even without passivation, improvements in the PD alone allow increasing the peak EPCE, PCE and IPCE to 85%, 96% and 105%, respectively. Fig. 8(c) shows that in the structure with an optimized PD and surface passivation, ELC can be directly observed for a wide range of input powers, from $\sim 1mW$ to $\sim 0.2W$ ($\sim 160mW/cm^2$ to $\sim 32W/cm^2$). As for the LED PCE (IPCE), ELC takes place in the input power range from $\sim 0.2mW$ to $\sim 0.6W$ ($\sim 32mW/cm^2$ to $\sim 96W/cm^2$).

For further analysis of passivation effects, Fig. 8(b) shows an example on how partial surface passivation affects the PCE of the DDS, by varying the surface recombination velocity for the structure using the optimized PD with a 100nm n-GaAs layer. In this example, observing ELC is possible when v_{sr} has been reduced to $\sim 5\%$ of the reference value. For $v_{sr} = 0$, the PCE is approximately 108%. While Figs. 7(b) and 8(a) indicate that ELC can take place internally in the LED even in

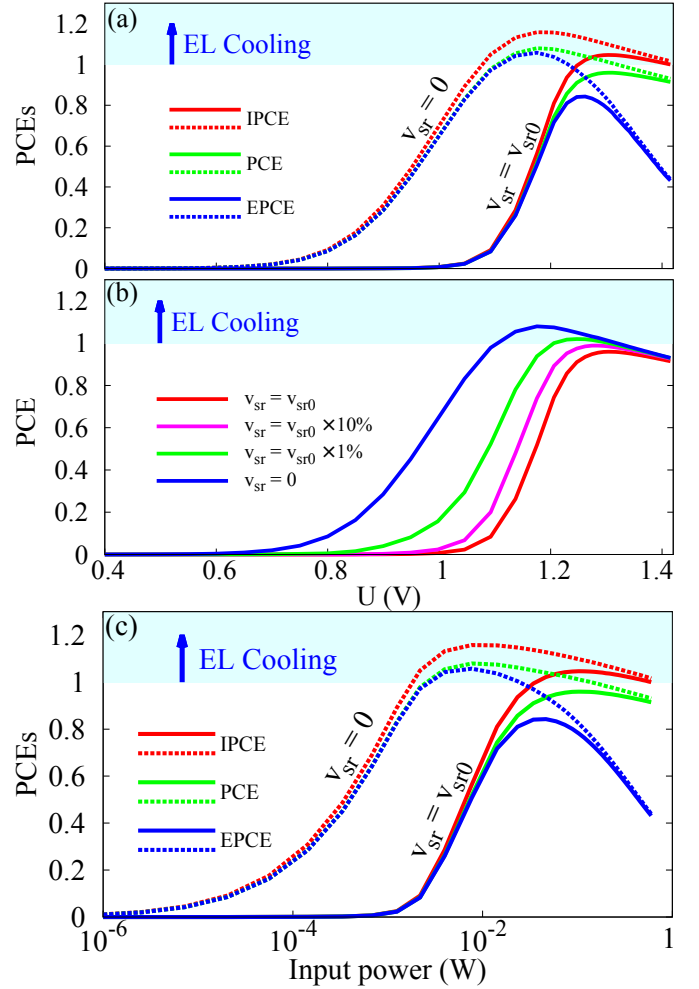


Fig. 8. The EPCE, PCE and IPCE as a function of (a) U and (c) the input power, for the reference (unpassivated) structure and the surface passivated structure ($v_{sr} = 0cm/s$). (b) The PCE as a function of U , for selected values of surface recombination velocity. The results are from the optimized photodetector structure using a 100nm n-type GaAs layer.

the presence of strong surface recombination, the net cooling of the LED only occurs if efficient passivation is achieved. The most basic traditional GaAs passivation techniques can easily reduce v_{sr} by more than one order of magnitude [26], [27], while epitaxially grown cap layers (e.g. III-P) [28] could ideally bring the values down to the 1.5 cm/s ($<0.001\%$) level [22]. Hence, it is expected that various efficient passivation techniques, ranging from atomic layer deposition to controlled oxidation [29] and epitaxial regrowth of III-P layers [30], can be developed and exploited to make use of ELC. Equivalently, it is expected that surface recombination can be eliminated by electrically isolating the surface, e.g. by eliminating the p-type conducting channel to the surface. Therefore it seems likely that the surface recombination can be pushed to well below the 1% limit shown in Fig. 8(b).

V. CONCLUSIONS

To conclude, we studied the possibility of demonstrating electroluminescent cooling in III-As based intracavity double diode structures (DDSs) at high powers and at room temperature. For a thorough analysis of the device physics

and performance, we combined experimental results with a calibrated electro-optical device simulation model. Our results indicate that the bulk properties of the III-V materials forming the DDS are already sufficient for achieving LED EL cooling at high powers, and that direct EL cooling observation through the DDS at such powers is feasible if surface recombination at the mesa edges are minimized and the detection efficiency of the photodetector integrated in the DDS is improved. In particular, our results also indicate that the LED power conversion efficiency of the studied setup can reach values larger than 115%, with LED EL cooling taking place over a wide range of input power densities, extending all the way up to $\sim 96\text{W}/\text{cm}^2$, if we suppress non-radiative surface recombination at the LED mesa walls, and radiative recombination in the PD by optimizing the PD layer structure.

ACKNOWLEDGMENT

We acknowledge funding from the Academy of Finland and the European Research Council under the Horizon 2020 research and innovation programme (grant No 638173).

REFERENCES

- [1] K. Lehovec, C. A. Accardo, and E. Jamgochian, "Light emission produced by current injected into a green silicon-carbide crystal," *Phys. Rev.*, vol. 89, pp. 20–25, Jan 1953, DOI: 10.1103/PhysRev.89.20.
- [2] J. Tauc, "The share of thermal energy taken from the surroundings in the electro-luminescent energy radiated from a p-n junction," *Czechoslovak Journal of Physics*, vol. 7, no. 3, pp. 275–276, May 1957, DOI: 10.1007/BF01688028.
- [3] R. J. Keyes and T. M. Quist, "Recombination radiation emitted by gallium arsenide," *Proceedings of the IRE*, vol. 50, no. 8, pp. 1822–1823, May 1962, DOI: 10.1109/JRPROC.1962.288223.
- [4] T. Patrick Xiao, K. Chen, P. Santhanam, S. Fan, and E. Yablonovitch, "Electroluminescent refrigeration by ultra-efficient GaAs light-emitting diodes," *Journal of Applied Physics*, vol. 123, no. 17, pp. 173 104–1–15, May 2018, DOI: 10.1063/1.5019764.
- [5] Z. Li, J. Xue, and R. Ram, "A design of a PhC-enhanced LED for electroluminescence cooling," R. I. Epstein, D. V. Seletskiy, and M. Sheik-Bahae, Eds. In Proc. SPIE Optical and Electronic Cooling of Solids II, Feb. 2017, pp. 1 012 108–1–10, DOI: 10.1117/12.2253403.
- [6] P. Santhanam, D. J. Gray, and R. J. Ram, "Thermoelectrically pumped light-emitting diodes operating above unity efficiency," *Physical Review Letters*, vol. 108, no. 9, pp. 097 403–1–5, Feb. 2012, DOI: 10.1103/PhysRevLett.108.097403.
- [7] P. Santhanam, D. Huang, R. J. Ram, M. A. Remennyi, and B. A. Matveev, "Room temperature thermo-electric pumping in mid-infrared light-emitting diodes," *Applied Physics Letters*, vol. 103, no. 18, pp. 183 513–1–5, Oct. 2013, DOI: 10.1063/1.4828566.
- [8] J. Xue, Y. Zhao, S.-H. Oh, W. F. Herrington, J. S. Speck, S. P. DenBaars, S. Nakamura, and R. J. Ram, "Thermally enhanced blue light-emitting diode," *Applied Physics Letters*, vol. 107, no. 12, pp. 121 109–1–5, Sep. 2015, DOI: 10.1063/1.4931365.
- [9] A. Olsson, J. Tiira, M. Partanen, T. Hakkarainen, E. Koivusalo, A. Tukiainen, M. Guina, and J. Oksanen, "Optical energy transfer and loss mechanisms in coupled intracavity light emitters," *IEEE Transactions on Electron Devices*, vol. 63, no. 9, pp. 3567–3573, Sep. 2016, DOI: 10.1109/TED.2016.2590461.
- [10] J. Tiira, I. Radevici, T. Haggren, T. Hakkarainen, P. Kivisaari, J. Lytikainen, A. Aho, A. Tukiainen, M. Guina, and J. Oksanen, "Intracavity double diode structures with GaInP barrier layers for thermophotonic cooling," R. I. Epstein, D. V. Seletskiy, and M. Sheik-Bahae, Eds. In Proc. SPIE Optical and Electronic Cooling of Solids II, Feb. 2017, pp. 1 012 109–1–7, DOI: 10.1117/12.2250843.
- [11] I. Radevici, J. Tiira, and J. Oksanen, "Lock-in thermography approach for imaging the efficiency of light emitters and optical coolers," R. I. Epstein, D. V. Seletskiy, and M. Sheik-Bahae, Eds. In Proc. SPIE Optical and Electronic Cooling of Solids II, Feb. 2017, pp. 101 210Q–1–7, DOI: 10.1117/12.2249978.
- [12] K. Chen, T. P. Xiao, P. Santhanam, E. Yablonovitch, and S. Fan, "High-performance near-field electroluminescent refrigeration device consisting of a GaAs light emitting diode and a Si photovoltaic cell," *Journal of Applied Physics*, vol. 122, no. 14, pp. 143 104–1–8, Oct. 2017, DOI: 10.1063/1.5007712.
- [13] J. Oksanen and J. Tulkki, "Thermophotonic heat pump—a theoretical model and numerical simulations," *Journal of Applied Physics*, vol. 107, no. 9, pp. 093 106–1–8, May 2010, DOI: 10.1063/1.3419716.
- [14] I. Radevici, J. Tiira, T. Sadi, and J. Oksanen, "Influence of photo-generated carriers on current spreading in double diode structures for electroluminescent cooling," *Semiconductor Science and Technology*, pp. 05LT01–1–5, Mar. 2018, DOI: 10.1088/1361-6641/aa66c3.
- [15] T. Sadi, P. Kivisaari, J. Tiira, I. Radevici, T. Haggren, and J. Oksanen, "Electroluminescent cooling in intracavity light emitters: modeling and experiments," *Optical and Quantum Electronics*, vol. 50, no. 1, pp. 18–1–8, Jan. 2018, DOI: 10.1007/s11082-017-1285-z.
- [16] P. Kivisaari, J. Oksanen, J. Tulkki, and T. Sadi, "Monte Carlo simulation of hot carrier transport in III-N LEDs," *Journal of Computational Electronics*, vol. 14, no. 2, pp. 382–397, Jun. 2015, DOI: 10.1007/s10825-015-0687-z.
- [17] J. Oksanen and J. Tulkki, "Effects of photon transport, emission saturation, and reflection losses on thermophotonic cooling," R. I. Epstein and M. Sheik-Bahae, Eds. In Proc. SPIE Laser Refrigeration of Solids IV, Feb. 2011, pp. 79 510H–1–7, DOI: 10.1117/12.873693.
- [18] T. Sadi, J. Oksanen, and J. Tulkki, "Improving light extraction from GaN light-emitting diodes by buried nano-gratings," *IEEE Journal of Quantum Electronics*, vol. 50, no. 3, pp. 141–147, Mar. 2014, DOI: 10.1109/JQE.2014.2299752.
- [19] Y. P. Varshni, "Band-to-band radiative recombination in groups IV, VI, and III-V semiconductors (I)," *phys. stat. sol. (b)*, vol. 19, no. 2, pp. 459–514, 1967, DOI: 10.1002/pssb.19670190202.
- [20] —, "Band-to-band radiative recombination in groups IV, VI, and III-V semiconductors (II)," *phys. stat. sol. (b)*, vol. 20, no. 1, pp. 9–36, 1967, DOI: 10.1002/pssb.19670200102.
- [21] U. Strauss, W. W. Rühle, and K. Köhler, "Auger recombination in intrinsic GaAs," *Appl. Phys. Lett.*, vol. 62, pp. 55–57, Jan. 1993, DOI: 10.1063/1.108817.
- [22] M. Levinstein, S. Rumyantsev, and M. Shur, [*Ternary And Quaternary III-V Compounds*], *Handbook Series on Semiconductor Parameters*. World Scientific Publishing, Nov. 1996, DOI: 10.1142/2046-vol2.
- [23] D. A. Bender, J. G. Cederberg, C. Wang, and M. Sheik-Bahae, "Development of high quantum efficiency GaAs/GaInP double heterostructures for laser cooling," *Appl. Phys. Lett.*, vol. 102, no. 25, pp. 252 102–1–4, Jun. 2013, DOI: 10.1063/1.4811759.
- [24] G. D. Gilliland, D. J. Wolford, T. F. Kuech, J. A. Bradley, and H. P. Hjalmarson, "Minority-carrier recombination kinetics and transport in surfacefree GaAs/Al_xGa_{1-x}As double heterostructures," *Journal of Applied Physics*, vol. 73, pp. 8386–8396, Feb. 1993, DOI: 10.1063/1.353407.
- [25] R. J. Nelson and R. G. Sobers, "Minority-carrier lifetimes and internal quantum efficiency of surfacefree GaAs," *Journal of Applied Physics*, vol. 49, pp. 6103–6108, Aug. 1978, DOI: 10.1063/1.324530.
- [26] A. G. Baca and C. I. H. Ashby, *Fabrication of GaAs Devices*. The Institution of Engineering and Technology, Jan. 2005, DOI: 10.1049/PBEP006E.
- [27] T. Ohno, "Sulfur passivation of GaAs surfaces," *Phys. Rev. B*, vol. 44, pp. 6306–6311, Sept 1991, DOI: 10.1103/PhysRevB.44.6306.
- [28] A. Aierken, "Passivation of GaAs surfaces and fabrication of self-assembled In(Ga)As/GaAs quantum ring structures," Ph.D. dissertation, Aalto University, 2008.
- [29] M. P. J. Punkkinen, P. Laukkanen, J. Lång, M. Kuzmin, M. Tuominen, V. Tuominen, J. Dahl, M. Pessa, M. Guina, K. Kokko, J. Sadowski, B. Johansson, I. J. Väyrynen, and L. Vitos, "Oxidized In-containing III-V(100) surfaces: Formation of crystalline oxide films and semiconductor-oxide interfaces," *Phys. Rev. B*, vol. 83, pp. 195 329–1–6, May 2011, DOI: 10.1103/PhysRevB.83.195329.
- [30] Y. Wada and K. Wada, "GaAs surface passivation by deposition of an ultrathin inp-related layer," *Appl. Phys. Lett.*, vol. 63, no. 3, pp. 379–381, 1993, DOI: 10.1063/1.110049.



Toufik Sadi received the M.Eng. degree in electronics from The University of Manchester, U.K., in 2004, and the Ph.D. degree in electronics from The University of Leeds, U.K., in 2008.

He is currently a Research Fellow with the Engineered Nanosystems Group, Aalto University, Finland. His current research interests include the theory, simulation, and characterization of semiconductor devices and circuits.



Ivan Radevici received the M.Sc. degree from Moldova State University, Moldova, in 2010, and the Ph.D. degree in semiconductor physics from the University of Turku, Finland, in 2015.

He is currently a Post-Doctoral Researcher with the Engineered Nanosystems Group, Aalto University, Finland. His research interests include growth, process, and characterization of semiconductor materials for optoelectronics and thermophotonics.



Pyry Kivisaari received the D.Sc. degree in computational science from Aalto University, Finland, in 2014.

He is currently an Academy of Finland Post-Doctoral Fellow with the Engineered Nanosystems Group, Aalto University. His research interests include modeling of optical and electrical transport in photonic devices and new devices based on diffusion-driven current transport.

Jani Oksanen Author's photograph and biography not available at the time of submission.